Correlations of Inhibitor Kinetics for Pneumocystis jirovecii and Human Dihydrofolate Reductase with Structural Data for Human Active Site Mutant Enzyme Complexes

ARTICLE *in* BIOCHEMISTRY · MARCH 2009

Impact Factor: 3.02 · DOI: 10.1021/bi801960h · Source: PubMed

6 AUTHORS, INCLUDING:

Vivian Cody
University at Buffalo, The State University of…
132 PUBLICATIONS **2,398** CITATIONS
SEE PROFILE

Jennifer Makin
State University of New York Upstate Medical…
2 PUBLICATIONS **36** CITATIONS
SEE PROFILE

Sherry F Queener
Indiana University-Purdue University Indiana…
228 PUBLICATIONS **4,866** CITATIONS
SEE PROFILE

Andre Rosowsky
Dana-Farber Cancer Institute
292 PUBLICATIONS **5,645** CITATIONS
SEE PROFILE

Published in final edited form as:
Biochemistry. 2009 March 3; 48(8): 1702–1711. doi:10.1021/bi801960h.

Correlations of Inhibitor Kinetics for *Pneumocystis jirovecii* and Human Dihydrofolate Reductase with Structural Data for Human Active Site Mutant Enzyme Complexes

Vivian Cody[1,2,*], **Jim Pace**[1], **Jennifer Makin**[1], **Jennifer Piraino**[1], **Sherry F. Queener**[3], and **Andre Rosowsky**[4]

[1] Structural Biology Department, Hauptman Woodward Medical Research Institute, 700 Ellicott St. Buffalo, New York 14203

[2] Structural Biology Department, School of Medicine and Biological Sciences, State University of New York at Buffalo, Buffalo, NY 14260

[3] Department of Pharmacology and Toxicology, Indiana University School of Medicine, Indianapolis, Indiana 46202

[4] Dana-Farber Cancer Institute, Harvard Medical School, Boston, MA 02115

Abstract

To understand the role of specific active site residues in conferring selective dihydrofolate reductase (DHFR) inhibition from pathogenic organisms such as *Pneumocystis carinii* (pc) or *Pneumocystis jirovecii* (pj), the causative agent in AIDS pneumonia, it is necessary to evaluate the role of these residues in the human enzyme. We report the first kinetic parameters for DHFR from pjDHFR and pcDHFR with methotrexate (MTX), trimethoprim (TMP), and its potent derivative, PY957. We also report the mutagenesis and kinetic analysis of active site mutant proteins at positions 35 and 64 of human (h) DHFR and the crystal structure determinations of four hDHFR ternary complexes of NADPH and PY957 with the wild type DHFR enzyme, the single mutant protein, Gln35Lys1, and two double mutant proteins, Gln35Ser/Asn64Ser and Gln35Ser/Asn64Phe. These substitutions place into human DHFR amino acids found at those sites in the opportunistic pathogens pcDHFR (Q35K/N64F) and pjDHFR (Q35S/N64S). The K_i inhibition constant for PY957 showed greatest potency of the compound for the N64F single mutant protein (5.2 nM), followed by wild type pcDHFR (K_i 22 nM), and then wild type hDHFR enzyme (K_i 230 nM). Structural data reveal significant conformational changes in the binding interactions of PY957 in the hDHFR Q35S/N64F mutant protein complex compared to the other hDHFR mutant protein complexes and the pcDHFR ternary complex. The conformation of PY957 in the wild type DHFR is similar to that observed for the single mutant protein. These data support the hypothesis that the enhanced selectivity of PY957 for pcDHFR is in part due to the in the design more selective inhibitors that target these opportunistic pathogens.

[1]The numbering used throughout this paper for the human DHFR sequence is based on the first position being Val-1 rather than Met-1 as observed in the gene sequence listing. This numbering has been used in previous publications of the kinetic and structural data for hDHFR and is being used here for continuity. unique contributions at positions 37 and 69 (pcDHFR numbering). This insight will help

*Author for correspondence. E-mail: cody@hwi.buffalo.edu, Phone: 716 898-8614, Fax: 716-898-8660.

Coordinates and crystallographic structure factors for human DHFR mutant complexes have been deposited in the Protein Data Bank under the accession codes: 3F8Y, 3F87, 3F91 and 3FS6.

Introduction

The atypical fungus *Pneumocystis jirovecii* (pj) is an opportunistic pathogen that causes life-threatening *Pneumocystis* pneumonia (PcP), one of the most prevalent opportunistic infections in patients with HIV AIDS (1–3). Current treatment of PcP combines the sulfa drug sulfamethoxazole with trimethoprim (TMP) (Fig. 1) that targets folate biosynthesis (1,4). Initial characterization of pjDHFR derived from patients with HIV AIDS (5) showed it was similar to *Pneumocystis carinii* (pcDHFR) found in rat lungs, but showed significant sequence differences (Table 1). These data also showed TMP was a weak competitive inhibitor with a K_i value of 2.8×10^{-7} M. In contrast, MTX was a tight-binding competitive inhibitor with a K_i of 1.6×10^{-11} M (5).

Recent studies have also shown the emergence of TMP drug resistance related to mutations in DHFR. For example, in a study of patients with PcP, some treated with a DHFR inhibitor and some with no prophylaxis, 19 DHFR nucleotide substitution sites were observed in 18 patients, with 16 of these sites giving rise to mutations (6). These data suggest that different *Pneumocystis jirovecii* populations with alternate forms of the target enzyme may arise with selective pressure from DHFR inhibitors.

Since *Pneumocystis jirovecii* cannot be grown in culture and will not reproduce in experimental animals, most drug design efforts have targeted DHFR from *Pneumocystis carinii* found in rat lungs (7–10). Although these two forms of DHFR are similar, they differ in their drug sensitivity. These differences provide an opportunity to design selective drugs that target a specific species of enzyme. This will of necessity require careful consideration of crucial differences in the active sites among these two fungal enzymes and human DHFR. Of note is the variability observed among the human and fungal enzyme sequences in the active site, in particular residues at positions 35 and 64 (hDHFR numbering, Table 1). In the human enzyme these residues are Gln and Asn, while in pcDHFR they are Lys and Phe, and Ser and Ser in pjDHFR. Structural data for inhibitor binding to h- or pcDHFR reveals that these residues interact with antifolates (11), and that inhibitors have been designed to target interactions with these residues (9–11).

In order to assess the role of active site variants among the pathogenic DHFR enzymes, whether as single or double mutant proteins, it is important to understand the role of these residues in giving rise to TMP resistance by weaker binding or in giving rise to enhanced native-like activity (12,13). In a study to screen for MTX-resistance of hDHFR, synergistic MTX-resistance could be obtained by combining two or more active-site mutations that confer weak MTX-resistance (12). In the combinatorial libraries that were created for positions 31, 34 and 35, mutations of Gln-35 were observed that reflected the residues for pc- and pjDHFR (i.e., Q35K, Q35S). Neither of these mutations caused MTX-resistance. Recent studies have also suggested that the effect of double mutants in an active site may be additive, partially additive, synergistic, antagonistic or absent (14).

Efforts to produce more selective and potent antifolates that target pcDHFR led to the design of novel 2,4-diamino-5-(ω-carboxy(alkyoxy) trimethoprim derivatives that showed 80–5000 fold increase in potency (IC_{50}) over the mammalian enzyme (15). We used PY957 (Fig. 1), a potent and selective compound from this series, to explore the critical differences in the active sites of mammalian and *Pneumocystis* DHFR. Herein we report the first kinetic analysis of recombinant pjDHFR, pcDHFR and hDHFR and for a larger series of active site mutants of hDHFR designed to explore sequence differences between the human and the two *Pneumocystis* enzymes (Tables 1–3), and the potent inhibitors, methotrexate (MTX), trimethoprim (TMP) and its derivative, PY957. Additionally, we report the crystal structures of human DHFR bearing the single amino acid substitution (Q35K) and hDHFR bearing two

double substitutions (Q35S/N64S and Q35S/N64F), as ternary complexes with NADPH and PY957. The crystal structure of PY957 with wild type pcDHFR has been reported (16). Taken together, these data enrich our understanding of the role of DHFR active site residues in conferring species selectivity and specificity of antifolate binding.

Experimental Procedures

Expression and Purification of pj- and pcDHFR

The cDNA for pj- or pcDHFR was transformed into *E. coli* Rosetta Gami B (DE3) competent cells with pET-SUMO-DHFR plasmid for expression. The general expression protocol is to inoculate a 10 ml culture of Luria broth (LB) containing ampicillin (AMP), grown overnight at 37°C, inoculate 1L of LB containing antibiotic and grow at 37°C to an OD_{600} of 0.6–0.8. The cells are then induced with isopropyl-β-D-thiogalactopyranoside (IPTG) at a final concentration of 1mM, shaken overnight at 16°C, and harvested by centrifugation at 4°C at 7000 rpm. The cell pellets were resuspended in a lysis buffer (100 ml of ice-cold buffer containing 6.8 g KH_2PO_4, 3.7g KCl, dissolved in 900 mL of H_2O, of 1.0 M ethylenediamine tetraacetic acid (EDTA) and pH adjusted to 7.0 with KOH before bringing the volume to 1L) and the cells broken using a microfluidzer at 18,000 psi (Microfluidics, Inc). The SUMO fusion protein has the His-tag for Ni-column purification which is removed by the SUMO protease (17), leaving a native protein. A two step purification protocol using a Ni-chelating IMAC for removal of the His-tagged protein, followed by Ulp1 protease cleavage, and passage over a second IMAC column resulted in a yield of 20–30 mg of purified enzyme from a liter of culture.

Construction and Expression of Mutant Human DHFR

Mutations were introduced into the cDNA of hDHFR and the entire coding sequence verified by Roswell Park Cancer Center (Buffalo, NY). DNA oligonucleotides were obtained from Integrated DNA Technologies (Coralville, IA) and used without further purification. Plasmid DNA was purified using the plasmid mini kit (Qiagen). Mutagenesis was performed using the QuikChange Site-Directed Mutagenesis Kit (Stratagene). All primers were PAGE purified and were synthesized by Alpha DNA (Montreal, Quebec) or IDT (Coralville, IA). Primers were designed according to manufacturer's recommendations as were the PCR reactions, with adjustments made for T_m of corresponding primers. PCR: (50 ng of dsDNA template, 100 ng of each primer, 5mM dNTPs, 2.5U/μL Taq) 1 cycle of 95°C for 30 sec, 16 cycles of 95°C for 30 sec, 55°C for 1 min, 68°C for 3 min.

Primers (5′ to 3′)

Q35K for: CAGATATTTCAAGAGAATGACCACAACC

Q35K rev: GGTTGTGGTCATTCTCTTGAAATATCTG

Q35S for: CAGATATTTCTCGAGAATGACCACAACC

Q35S rev: GGTTGTGGTCATTCTCGAGAAATATCTG

N64F for: GGTTCTCCATTCCTGAGAAGTTTCGACCTTTAAAGGGTAG

N64F rev: CTACCCTTTAAAGGTCGAAACTTCTCAGGAATGGAGAACC

N64S for: GGTTCTCCATTCCTGAGAAGAGTCGACCTTTAAAGGGTAG

N64S rev: CTACCCTTTAAAGGTCGACTCTTCTCAGGAATGGAGAACC

The original wild type human DHFR (pDS5 vector) was used for PCR and all subsequent mutagenesis experiments. Four single mutants were created (Q35K, Q35S, N64F, and N64S) with the QuikChange Site Directed Mutagenesis Kit following the manufacturer's recommended conditions. Four double mutant proteins (Q35K/N64F, Q35S/N64F, Q35K/N64S, Q35S/N64S) were created by using parental template DNA having one confirmed single residue mutation and using primers for the second desired mutation during PCR.

Expression and purification of human DHFR pDS5/mutant pDS5

The following protocol was used for expression of wild type (wt) human DHFR (18) and mutant human DHFR in pDS5 vector in *E. coli* BL21 (DE3): 200mL of LB medium containing 100ug/mL AMP was inoculated with glycerol stock of hDHFR at 37°C with shaking at 300 rpm overnight. One liter of fresh LB/AMP was inoculated with the 200mL culture overnight and grown at 37°C at 300 rpm until the $O.D._{600}$ 0.8–0.9. Cells were then induced with 2mM IPTG overnight at 16°C (16–18 hr) and harvested by centrifugation at 13,000 x g. Cells were resuspended in 100mL of ice-cold M9 salt solution (12.8g Na_2HPO_4-$7H_20$, 3g KH_2PO_4, 0.5g NaCl, 1g NH_4Cl in a volume of 1L).

Cells were lysed in 100mL of ice-cold buffer containing 6.8g KH_2PO_4, 3.7g KCl, dissolved in 900mL of H20, 1.0mL of 1.0M ethylenediamine tetra acetic acid (EDTA) was added and the pH adjusted to 7.0 with KOH before bringing volume to 1L. Cells were disrupted by passing through a microfluidizer at 18,000 psi (Microfluidics, Inc). The resulting lysate was subjected to centrifugation for 30 min. at 7,000 × g. Ammonium sulfate was added to supernatant over a period of 60 min. to a final saturation of 85% at 0°C. Precipitated protein was centrifuged for 30 min. at 7,000 × g and the pellet resuspended in 50mL of methotrexate column binding buffer (100mM KCl, 50mM K_2PO_4, pH 7.0). The resulting sample was passed over a 25mL methotrexate affinity column. The column was extensively washed (>5 column volumes of buffer) to remove unbound protein. DHFR was subsequently eluted in 5mL fractions by passing a solution of 4mM folic acid, 50mM potassium phosphate, pH 8.0 over the column. SDS-PAGE was performed on fractions to determine which contained DHFR. The corresponding fractions were then pooled and dialyzed extensively against DEAE column buffer (50mM K_2PO_4, pH 7.5) to remove folic acid from solution. On the following day the sample was applied to a 120mL DEAE ion exchange column (GE Healthcare). All fractions were analyzed by SDS-PAGE. Fractions containing highly pure (>95%) DHFR were pooled, concentrated to 1mg/mL, flash-frozen in liquid nitrogen, and stored at −80°C.

Kinetic Analysis

Standard DHFR assays were conducted using a standard 1 cm path-length cuvette at 37°C with continuous recording of change of OD at 340 nM. The assay contained 41 mM sodium phosphate buffer at pH 7.4, 2-mercaptoethanol 8.9 mM, 150 mM KCl, and saturating concentrations of NADPH and dihydrofolic acid (DHFA). With human DHFR, DHFA concentrations were 18 or 90 μM DHFA; 117 μM NADPH was used. The optimal level of DHFA for each protein was determined and selected to give maximal activity without approaching levels that might be inhibitory. Because K_i values take into account the amount of substrate in the assay, these differences do not affect the final value. Initial rates of enzyme activity were measured; rates were linear under standard conditions for about 5 minutes for human DHFR. Activity was linearly related to protein concentration under these conditions of assay.

K_m values were determined by holding either substrate or cofactor at a constant, saturating concentration and varying the other over a range of concentrations. The K_m value was determined by fitting the data to the Michaelis-Menten equation using nonlinear regression

methods (Prism 4.0). The value of k_{cat} was determined from the Vmax value and the protein concentration ($k_{cat} = V_{max}$[Etot]) (Table 2).

K_i values were determined by measuring inhibition of the reaction at two or more concentrations of substrate (DHFA). For the competitive inhibitors such as trimethoprim, K_i could be calculated from the equation:

$$K_i = IC_{50}/(1+S/K_m)$$

Methotrexate followed the pattern of a tight-binding inhibitor (18) and PY957 inhibition best fit a linear mixed model (19).

All determinations of IC_{50} were made by fitting percent inhibition data to a single site sigmoidal model with variable slope, using nonlinear regression methods (Prism 4.0). All inhibition curves required at least four points within the central segment of the sigmoidal curve. Statistical comparisons were preformed with InStat 2.03, using the nonparametric Welch t test because variances among groups could not be shown to be equal; this test is more conservative than the standard t test. These results are shown in Table 3. The values in the tables represent mean plus/minus standard error of the mean when replicates are 3 or more; when n =1 or 2, the values are the mean plus/minus standard error for the curve fitting. Additional graphical representations of these kinetic data are illustrated in Figs. 1S and 2S of the supplementary material.

Crystallization

Buffers for the Q35K single mutant protein and the Q35S/N64F and Q35S/N64S double mutant proteins of human DHFR were exchanged in a centricon 10,000 MWCO filter with 100 mM K_2PO_4 buffer, pH 6.9 and concentrated to 4.2 mg/mL for the single mutant protein and 6.6 mg/mL for the double mutant proteins of hDHFR. The protein was incubated with NADPH and a 10:1 molar excess of the inhibitor, PY957, for one hour over ice prior to crystallization using the hanging drop vapor diffusion method using siliconized glass cover slips. The 10 μL protein droplets that contained a final protein buffer of 100 mM K_2PO_4, pH 6.9 with 30% saturated ammonium sulfate were suspended over a reservoir solution of 100 mM K_2PO_4, pH 6.9, 60% saturated ammonium sulfate with 3% v/v ethanol. Samples were stored at 14°C and crystals grew in about three days and were trigonal, space group R3 in the H3 hexagonal setting.

A data set for the single Q35K mutant protein hDHFR ternary complex was collected on a Rigaku RaxisIV imaging plate system with MaxFlux optics to 1.8Å resolution and a second, higher resolution data set was collected to 1.45Å resolution using the remote access protocol on beam line 9–1 at the Stanford Synchrotron Radiation Laboratory (SSRL) facility (20–22). Only data from SSRL are reported for the single mutant. Data for the wild type hDHFR ternary complex with PY957 and NADPH were also collected to 1.2Å resolution on beam line 9–2 at SSRL. Data were collected on the Rigaku RaxisIV imaging plate system to 1.90–2.0Å resolution for the two double mutants of the hDHFR ternary complex with NADPH and PY957. All data were processed using Mosflm (23). Diffraction statistics are shown in Table 4 for all complexes.

Structure Determination

The structures were solved by molecular replacement methods using the coordinates for wild type human DHFR (1U72) (24) in the program Molref (23). Inspection of the resulting difference electron density maps were made using the program COOT (25) running on a Mac G5 workstation and revealed density for a ternary complex for all structures (Fig. 2a–c). To monitor the refinement, a random subset of all reflections was set aside for the calculation of

Rfree (5%). The model for the inhibitor was taken from the coordinates of the pcDHFR NADPH PY957 ternary complex (16). The parameter file for the cofactor and inhibitor were prepared using the Dundee PRODGR2 Server website (http://davapc1.bioch.dundee.ac.uk/programs/prodrg) (26). The final cycles of refinement were carried out using the program Refmac5 in the CCP4 suite of programs (23). The Ramachandran conformational parameters from the last cycle of refinement generated by PROCHECK (27) showed that more than 90% of the residues in all complexes have the most favored conformation and none are in the disallowed regions (Table 4). Coordinates for these structures have been deposited with the Protein Data Bank (accession numbers 3f8y, 3f87, 3f91 and 3fs6 for the hDHFR structures listed in Table 4).

Results

Steady State Kinetic Parameters

The parameters reported in Table 2 give the overall effect of mutations on catalytic activity. There is no significant departure from Michaelis-Menten kinetics observed for any of the variants. The K_m values for DHFA and NADPH for hDHFR (Table 2) are somewhat greater than previously reported values of 0.12 μM and 0.16 μM, respectively, (28–31); however, our values were determined at 37°C in the presence of 150 mM KCl and the cited values were measured at 20°C in the presence of NaCl, which likely accounts for the differences. The data in Table 2 show K_m values for DHFA are similar for pjDHFR, hDHFR, and its mutant proteins Q35S and Q35S/N64S. The mutant proteins Q35K, N64S, N64F, and Q35K/N64F all have lower K_m values for DHFA than either wild type human or wild type pcDHFR. The values of k_{cat} previously reported for hDHFR range from 6.9 to 11 sec^{-1}, assayed at 20°C (28–31), and are generally in line with the value of 40 sec^{-1} we measured at 37°C. The value of k_{cat} is not significantly affected by any of the mutations studied.

Inhibition of hDHFR variants by antifolates

The K_i for all variants at positions 35 and 64 were determined for TMP, MTX and PY957 (Table 3). Mutant protein for N64S DHFR had a K_i value for MTX statistically significantly lower than that of hDHFR. Mutant protein Q35S hDHFR and Q35S/N64S showed K_i values for MTX that were identical to the value for pjDHFR but were not statistically significantly lower than the K_i for hDHFR. In contrast, all mutant proteins converting hDHFR to a more pc-like active site (Q35K, N64F, Q35K/N64S) showed values near that of wild type pcDHFR and were statistically lower than the value for hDHFR.

K_i values for TMP are in general agreement with the values reported from enzyme taken from AIDS patients (Table 3) (5). The K_i values for TMP were statistically significantly lower than the value for hDHFR in the Q35S, N64S, and Q35S/N64S mutant protein series, but were not as low as the value for native pjDHFR. In contrast, hDHFR mutants Q35K, N64F, and Q35K/N64F showed K_i values that were statistically lower than the value for hDFHR but not significantly different than the value for pcDHFR. These results suggest that the selectivity of interaction of TMP with DHFR depends heavily on the residues at positions 35 and 64. However, structural data reported for the ternary complex of pcDHFR with NADPH and TMP indicate few interactions of TMP with Lys37 and Phe69 (32).

The K_i values for PY957 follow a pattern similar to that of its homolog TMP: mutant Q35S/N64S has a K_i value lower than hDHFR but higher than pjDHFR, and all K_i values for mutant hDHFR with pcDHFR substitutions (Q35K, N64F, Q35K/N64F) are significantly lower than the value for hDHFR, but not significantly different from the K_i for pcDHFR. These results suggest that PY957 exploits some of the same interactions as TMP to achieve selectivity.

Overall Structure and Ligand Binding Conformation

The Q35S/N64S doubly substituted mutant protein hDHFR was designed to make the active site of the human enzyme more like the active site of pjDHFR while the single Q35K single mutant protein makes that position like that of the pcDHFR active site, whereas the Q35S/N64F double mutant protein is a cross between the pc- and pjDHFR sequences at these positions. Overall, the structures of these mutant proteins resemble those previously reported for hDHFR, and preserve the previously reported hydrogen bond network involving structural water, the conserved residues Thr136, Trp24, Glu30, and the N1 nitrogen and 2-amino group of PY957 (28–30). Similarly, the 4-amino group of PY957 maintains contact with the conserved residues Ile7 and Tyr121 and NADPH. The binding orientation of the diaminopyrimidine ring of PY957 is similar to that observed in the pcDHFR ternary structure (16).

The conformation of PY957 in the hDHFR wild type and mutant protein complexes differs significantly from that observed in the pcDHFR ternary inhibitor complex (Fig. 5) (16). Comparison of the torsion angle rotation about the C5-C51 and C51-C1′ bonds (Fig. 1,Table 5) reveals that the two ring systems are mutually perpendicular, unlike that observed in the pcDHFR complex (16). This conformation of PY957 in the hDHFR mutant protein complexes positions the 2′-methoxy carbon such that it makes hydrophobic contact with the methyl carbon of Thr56 (3.0, 3.5, and 3.4Å, for the single Q35K and double Q35S/N64F and Q35S/N64S mutants, respectively), with the side chain of Val115 (4.1, 3.7 and 3.7 Å), and to the nicotinamide ring of NADPH (3.6, 4.0 and 3.8 Å). The 2′-methoxy oxygen makes contact with the backbone carbonyl of Val115 (3.4, 3.8 and 3.7 Å, respectively). In the pcDHFR complex with PY957 (16), these contacts are to Leu25 (4.0 Å), Thr61 (4.8 Å), and to the nicotinamide ring (3.7 Å).

There are also significant differences in the conformation among the “(5′-ω-carboxyalkyoxy)” side chains of PY957 observed in all the variant complexes of hDHFR (Table 5 and Fig. 3). In the Q35K structure that has Lys35 and Asn64 in the binding pocket, the methylene carbons of the side chain of PY957 are extended and make weak hydrophobic contacts to the Lys35 and Asn64 (3.9–4.8 Å). In the case of the Q35S/N64S double mutant, these residues are both Ser and the side chain methylene carbons are folded such that they are closer to Leu60 and Ser59 (3.3–4.3 Å, respectively) (Fig. 3). In the cross-species variant Q35S/N64F, the side chain conformation has changed significantly and is positioned between Phe31 and Phe64 rather than forming interactions with the conserved Arg70 as in the other mutant structures (Fig. 4). The corresponding residue in pcDHFR is Phe69 (pcDHFR numbering), that can contribute strong hydrophobic interactions to the methylene carbons of the inhibitor side chain (16). Thus, although the two mutant hDHFR forms and pcDHFR differ in the way they interact with the methylene carbons in the side chain of PY957, the single Q35K and Q35S/N64S double mutants retain these interactions in some form.

The position of the side chain of the conserved Arg70 is maintained by a network of hydrogen bond contacts from the side chains of residues Thr38 and Thr39 and from the backbone functional groups of Lys68 (16). As expected, the carboxylate group of PY957 forms close contacts to the conserved Arg70 in hDHFR Q35K and Q35S/N64S variant complexes; however, in the case of the Q35S/N64F double mutant, there is an unexpected change in the inhibitor side chain conformation such that it no longer makes contact with Arg70. In this complex, the inhibitor carboxylate interactions are replaced by water molecules (Fig. 2c). The carboxylate oxygen atoms of PY957 in this alternate conformation make weak interactions with water molecules near the surface of the enzyme. The side chain may be disordered as the B values for thermal motion for the methylene carbons of the side chain are nearly twice (about 30) those in the remaining structure.

In all the mutant protein DHFR structures, NADPH is fully occupied and is bound in an extended conformation similar to other DHFR cofactor complexes (11,16). In the case of the wild type hDHFR ternary complex, the cofactor is partially occupied in the extended conformation. The carboxamide group of the nicotinamide rings, which is syn to the nicotinamide ring N, makes a series of strong hydrogen bonds with the backbone carbonyls of the conserved residues Ile7, Val115 in hDHFR. The conserved cis peptide linkage between the invariant Gly117 and Gly118 permits the pyrophosphate oxygen atoms of the cofactor to interact.

Discussion

This is the first report of the kinetic and structural parameters for the pjDHFR and for the single and double variants at positions 35 and 64 of hDHFR that make the human enzyme resemble the DHFR from the two opportunistic pathogens from *Pneumocystis*, i.e., Q35K and N64F for human to pcDHFR, and Q35S and N64S for human to pjDHFR. Structural data suggest that binding of PY957 is qualitatively different among pcDHFR, Q35S/N64F, Q35S/N64S hDHFR, and Q35K hDHFR. Likewise, the kinetic data shows differences in K_i values for these three enzyme forms: Q35K hDHFR has the lowest K_i for PY957 (8.3 ± 0.4 nM), followed by pcDHFR (21.9 ± 9.3 nM) and Q35S/N64S hDHFR (66 ± 2 nM) and these values are statistically different from one another.

Converting key active site residues at positions 35 and 64 of the human DHFR to amino acids found at these analogous sites in *P. jirovecii* or *P. carinii* DHFR had little effect on k_{cat}. This result is rational, considering that selective pressure during evolution would be presumed to preserve catalytic activity of this important metabolic enzyme; however, the mutations at positions 35 and 64 of the human enzyme do show a small effect on the K_m for DHFA. The single and double mutants introducing *P. carinii* residues into the human enzyme at positions 35 and 64 show a statistically lower K_m for substrate DHFA than the native human enzyme; the same tendency is seen for the *P. jirovecii* residues but the effect is not statistically significant.

Given that our steady state conditions for determining K_m were with saturating concentrations of NADPH, the enzyme reaction scheme simplifies to:

$$E+S \underset{k_{-1}}{\overset{k_1}{\longleftrightarrow}} ES \xrightarrow{k_{cat}} E+P$$

and thus K_m is defined as $(k_{-1} + k_{cat})/k_1$. Our determinations of k_{cat} show it to be unchanged in the mutants studied. Therefore, lowered K_m values must reflect either a decreased k_{-1} value, or an increased k_1 value, or both; in either case, the suggestion is that these mutations affect affinity of the substrate for the active site. Therefore, if we use an array of substrate analogs to probe the active sites of native and mutant forms of DHFR, we would expect to see significant differences in K_i, the equilibrium dissociation constant for binding (k_{-1}/k_1).

For the competitive inhibitor TMP, our results agree with the above prediction, in that we saw improved affinity for TMP (lower K_i) in all mutants. For the series of mutants converting human to *P. jirovecii*-like residues at positions 35 and 64, the changes in K_i values relative to those of native human enzyme were: Q35S, 2.89-fold reduction; N64S, 30.59-fold reduction; Q35SN64S, 4.33-fold reduction. Using the reasoning suggested by Mildvan (14), these values may be converted to log form: Q35S, $10^{0.46}$, N64S $10^{1.49}$, Q35SN64S $10^{0.64}$. The effects of the two residues are clearly not additive (i.e., $10^{1.95} \neq 10^{0.64}$), suggesting that the residues do not act independently in affecting TMP binding. For mutant proteins converting hDHFR to a more *P. carinii*-like active site, the log values of changes are: Q35K $10^{1.12}$, N64F $10^{1.03}$, Q35K/

N64F $10^{0.9}$. The mutations Q35S and N64S are neither additive nor synergistic, but rather the presence of Q35S seems capable of reversing the effects of N64S; reversal of the effects on K_i is complete or nearly complete for MTX and TMP, but only partial for PY957. Similar analysis based on the K_i values for the pseudo-irreversible inhibitor MTX and the linear mixed inhibitor PY957 also suggest a degree of antagonism in both sets of mutants, i.e. the effect on the double mutant is less than the effect seen for one or both of the single mutants.

These data are consistent with the structural results observed for the single and double mutants bound with PY957. In these structures, variations in the side chain conformation reflect differences in its interactions with the mutants at positions 35 and 64 in the hDHFR ternary complexes with PY957 while maintaining the strong interactions of the inhibitor carboxylate with Arg70. The conformation of the PY957 side chain in the Q35S/N64F double mutant protein complex was unexpected as the side chain of PY957 flips away from Arg70 and instead the methylene carbons of the side chain form hydrophobic interactions with Phe31 and Phe64 (Fig. 4). The carboxylate oxygen atoms of PY957 in this orientation make weak interactions with water molecules on the surface of the enzyme.

Structural data for the binding of PY957 to the hDHFR variants and to pcDHFR provide insight into the contribution of the active site residues at positions 35 and 64 to the selectivity and specificity of inhibitor binding to h-, pc- and pjDHFR. These data show that the conformation of the "5-(ω-carboxyalkyoxyl)" side chain of PY957 is flexible and can adopt conformations that optimize its binding interactions with the residues that line the active site. These data suggest that the interactions with side chains of residues at position 64 may contribute more to inhibition than those at position 35 as indicated by the alternative side chain conformation observed in the structure of the Q35S/N64F double mutant of hDHFR. These results imply that the hydrophobic contributions to binding by contacts to Phe31 and Phe64 by the PY957 side chain are greater than those made by the interactions of Ile33 and Phe69 in the pcDHFR ternary complex with PY957 (16). Since Ile33 is smaller than Phe31, it can not make the same contribution to hydrophobic binding as observed in the Q35S/N64F human complex. Although the PY957 side chain can interact electrostatically with Arg75 in the pcDHFR ternary complex, the side chain conformation changes to enhance its hydrophobic interactions with Phe69 and may result in the twisting of the torsion angle between the two ring systems of PY957 as a consequence of this interaction.

The relationships between specificity of PY957 inhibitory potency and active site mutations in hDHFR correlate with the conformational patterns observed in PY957 binding and the enhanced binding observed for those variants that make these active site positions more like those of the *Pneumocystis* DHFR enzymes.

These results taken together suggest that PY957 interacts with the DHFR enzymes from *Pneumocystis* in ways that are different from TMP such that binding is enhanced (lower K_i) and selectivity is still achieved. This conclusion is supported by the observation that TMP binding follows the pattern of classical competitive inhibition (only K_m affected), whereas PY957 best fits a model of linear mixed inhibition (both K_m and Vmax affected).

These data validate the hypothesis that the increased selectivity of PY957 for pcDHFR is in part due to contributions of the species specific residues Lys37 and Phe69 of pcDHFR. This insight into the contribution of species-specific residues to inhibitor binding will help in the design of more selective inhibitors that target specific opportunistic fungal pathogens.

Supplementary Material

Refer to Web version on PubMed Central for supplementary material.

Acknowledgments

This work was supported in part by a grant from the National Institutes of Health, GM51670 (VC).

The authors thank the beam line staff at SSRL for their support. Portions of this research were carried out at the Stanford Synchrotron Radiation Laboratory, a national user facility operated by Stanford University on behalf of the U.S. Department of Energy, Office of Basic Energy Sciences. The SSRL Structural Molecular Biology Program is supported by the Department of Energy, Office of Biological and Environmental Research and by the National Institutes of Health, National Center for Research Resources, Biomedical Technology Program, and the National Institute of General Medical Sciences. The authors also thank Dr. Edward Snell for his help in data collection and processing.

Abbreviations

DHFR
: dihydrofolate reductase

DHFA
: dihydrofolic acid

pj
: *Pneumocystis jirovecci*

pc
: *Pneumocystis carinii*

IC_{50}
: concentration giving 50% inhibition

K_i
: inhibition constant for inhibition

References

1. Kovacs JA, Gill VJ, Meshnick S, Masur H. New Insights into Transmission, Diagnosis, and Drug Treatment of *Pneumocystis carinii* Pneumonia. J Amer Med Assoc 2001;286:2450–2460.
2. Hughes WT. Prevention and Treatment of *Pneumocystis carinii* Pneumonia. Ann Rev Med 1991;42:287–295. [PubMed: 2035974]
3. Totet A, Duwat H, Magois E, Jounieaux V, Roux P, Raccurt C, Nevez G. Similar Genotypes of *Pneumocystis jirovecii* in Different Forms of *Pneumocystis* Infection. Microbiology 2004;150:1173–1178. [PubMed: 15133077]
4. Benfield T, Atzori C, Miller RF, Helweg-Larsen J. Second-Line Salvage Treatment of AIDS-Associated *Pneumocystsis jirovecii* Pneumonia. J Acquir Immune Defic Syndr 2008;48:63–67. [PubMed: 18360286]
5. Ma L, Kovacs JA. Expression and Characterization of Recombinant Human-derived *Pneumocystis carinii* Dihydrofolate Reductase. Antimicrob Agents Chemother 2000;44:3092–3096. [PubMed: 11036028]
6. Nahimana A, Rabodonirina M, Bille J, Francioli P, Hauser PM. Mutations of *Pneumocystis jirovecii* Dihydrofolate Reductase Associated with Failure of Prophylaxis. Antimicrobial Agents Chemother 2004;48:4301–4305.
7. Chan DCM, Anderson AC. Towards Species-Specific Antifolates. Current Med Chem 2006;13:377–398.
8. Gangjee A, Jain H, Kurup S. Recent Advances in Classical and Non-classical Antifolates as Antitumor and Antiopportunistic Infection Agents, Part I. Anticancer Agents Med Chem 2007;7:523–542.
9. Gangjee A, Jain H, Kurup S. Recent Advances in Classical and Nonclassical Antifolates as Antitumor and Antiopportunistic Infection Agents, Part II. Anticancer Agents Med Chem 2008;8:205–231. [PubMed: 18288923]

10. Gangjee A, Kurup S, Namjoshi O. Dihydrofolate Reductase as a Target for Chemotherapy in Parasites. Curr Pharm Des 2007;13:609–639. [PubMed: 17346178]
11. Cody V, Schwalbe CH. Structural Characteristics of Antifolate Dihydrofolate Reductase Enzyme Interactions. Crystallographic Reviews 2006;12:301–333.
12. Volpato JP, Fossati E, Pelletier JN. Increasing Methotrexate Resistance by Combination of Active-site Mutations in Human Dihydrofolate Reductase. J Mol Biol 2007;373:599–611. [PubMed: 17868689]
13. Fossati E, Volpato JP, Poulin L, Guerrero V, Dugas DA, Pelletier JN. 2-Tier Bacterial and In Vitro Selection of Active and Methotrexate-Resistant Variants of Human Dihydrofolate Reductase. J Biomol Screen 2008;13:504–514. [PubMed: 18566481]
14. Mildvan AS. Inverse Thinking About Double Mutants of Enzymes. Biochemistry 2004;43:14517–145120. [PubMed: 15544321]
15. Rosowsky A, Forsch RA, Queener SF. Further Studies on 2,4-Diamino-5-(2′,5′-disubstitutedbenzyl) pyrimidines as Potent and Selective Inhibitors of Dihydrofolate Reductases from Three Major Opportunistic Pathogens of AIDS. J Med Chem 2003;46:1726–1736. [PubMed: 12699390]
16. Cody V, Pace J, Chisum K, Rosowsky A. New Insights into DHFR Interactions: Analysis of *Pneumocystis carinii* and Mouse DHFR Complexes with NADPH and Two Highly Potent 5-(ω-Carboxy(alkyloxy)) Trimethoprim Derivatives Reveals Conformational Correlations with Activity and Novel Parallel Ring Stacking Interactions. Proteins: Structure, Function and Bioinformatics 2006;65:959–969.
17. Mossessova E, Lima CD. Ulp1-SUMO Crystal Structure and Genetic Analysis Reveal Conserved Interactions and a Regulatory Element Essential for Cell Growth in Yeast. Molecular Cell 2000;5:865–876. [PubMed: 10882122]
18. Appleman JR, Prendergast N, Delcamp TJ, Freisheim JH, Blakley RL. Kinetics of the Formation and Isomerization of Methotrexate Complexes of Recombinant Human Dihydrofolate Reductase. J Biol Chem 1988;263:10304–10313. [PubMed: 3292526]
19. Segel IH. Enzyme Kinetics: Behavior and Analysis of Rapid Equilibrium and Steady-State Enzyme Systems. Wiley-Interscience. 1975(957 pages)
20. McPhillips TM, McPhillips SE, Chiu HJ, Cohen AE, Deacon AM, Ellis PJ, Garman E, Gonzalez A, Sauter NK, Phizackerley RP, Soltis SM, Kuhn P. Blu-Ice and the Distributed Control System: Software for Data Acquisition and Instrument Control at Macromolecular Crystallography Beamlines. J Synchrotron Rad 2002;9:401–406.
21. Cohen AE, Ellis PJ, Miller MD, Deacon AM, Phizackerley RP. An Automated System to Mount Cryo-cooled Protein Crystals on a Synchrotron Beamline, Using Compact Sample Cassettes and a Small-scale Robot. J Appl Cryst 2002;35:720–726.
22. Gonzalez A, Moorhead P, McPhillips SE, Song J, Sharp K, Taylor JR, Adams PD, Sauter NK, Soltis SM. Web-Ice: Integrated Data Collection and Analysis for Macromolecular Crystallography. J Appl Cryst 2008;41:176–184.
23. Collaborative Computational Project, Number 4, The CCP4 Suite: Programs for Protein Crystallography. Acta Crystallogr 1994;D50:760–763.
24. Cody V, Luft JR, Pangborn W. Understanding the Role of Leu22 Variants in Methotrexate Resistance: Comparison of Wild-type and Leu22Arg Variant Mouse and Human Dihydrofolate Reductase Ternary Crystal Complexes with Methotrexate and NADPH. Acta Cryst 2005;D61:147–155.
25. Emsley P, Cowtan K. Coot: Model-Building Tools for Molecular Graphics. Acta Cryst 2004;D60:2126–2132.
26. Schuettelkopf AW, van Aalten DMF. PRODRG A Model Tool for High-throughput Crystallography of Protein-ligand Complexes. Acta Cryst 2004;D60:1355–1363.
27. Laskowski RA, MacArthur MW, Moss DS, Thornton JM. PROCHECK: A Program to Check the Stereochemical Quality of Protein Structure. J Applied Cryst 1993;26:283–291.
28. Chunduru SK, Cody V, Luft JR, Pangborn W, Appleman JR, Blakley RL. Methotrexate-resistant Variants of Human Dihydrofolate Reductase: Effects of Phe31 Substitutions. J Biol Chem 1994;269:9547–9555. [PubMed: 8144541]
29. Lewis WS, Cody V, Galitsky N, Luft JR, Pangborn W, Chunduru SK, Spencer HT, Appleman JR, Blakley RL. Methotrexate-resistant Variants of Human Dihydrofolate Reductase with Substitutions

of Leucine 22: Kinetics, Crystallography and Potential as Selectable Markers. J Biol Chem 1995;270:5057–5064. [PubMed: 7890613]

30. Cody V, Luft JR, Pangborn W, Gangjee A. Analysis of Three Crystal Structure Determinations of a 5-Methyl-6-N-Methylanalino Pyridopyrimidine Antifolate Complex with Human Dihydrofolate Reductase. Acta Cryst 2003;D59:1603–1609.
31. Appleman JR, Beard WA, Delcamp TJ, Prendergast NJ, Freisheim JH, Blakley RL. Unusual Transient- and Steady-state Kinetic Behavior is Predicted by the Kinetic Scheme Operational for Recombinant Human Dihydrofolate Reductase. J Biol Chem 1990;265:2740–2748. [PubMed: 2303423]
32. Champness JN, Achari A, Ballantine SP, Bryant PK, Delves CJ, Stammers DK. The Structure of *Pneumocystis carinii* Dihydrofolate Reductase to 1.9Å Resolution. Structure 1994;2:915–924. [PubMed: 7866743]
33. DeLano Scientific LLC., PyMol.

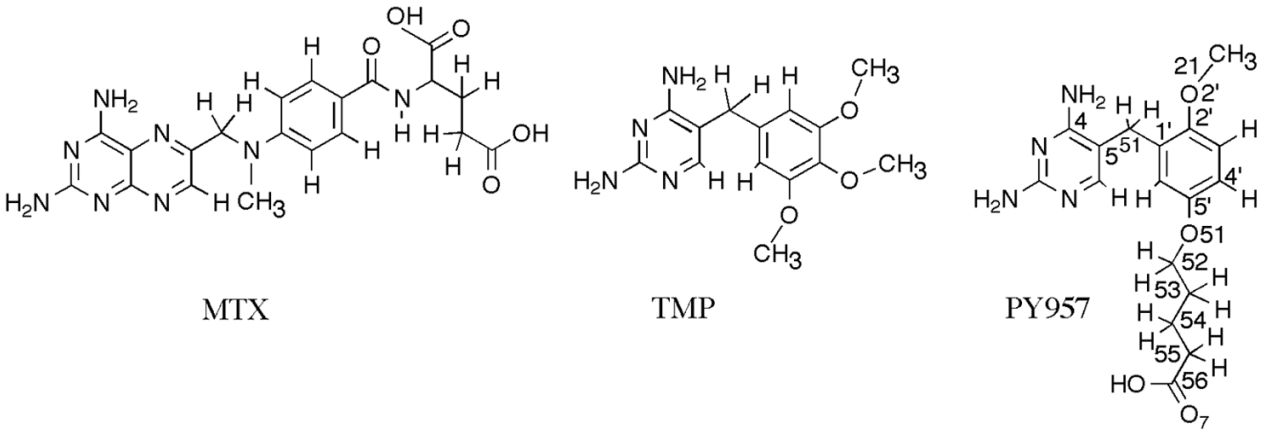

Figure 1.
Schematic representation of antifolates under study.

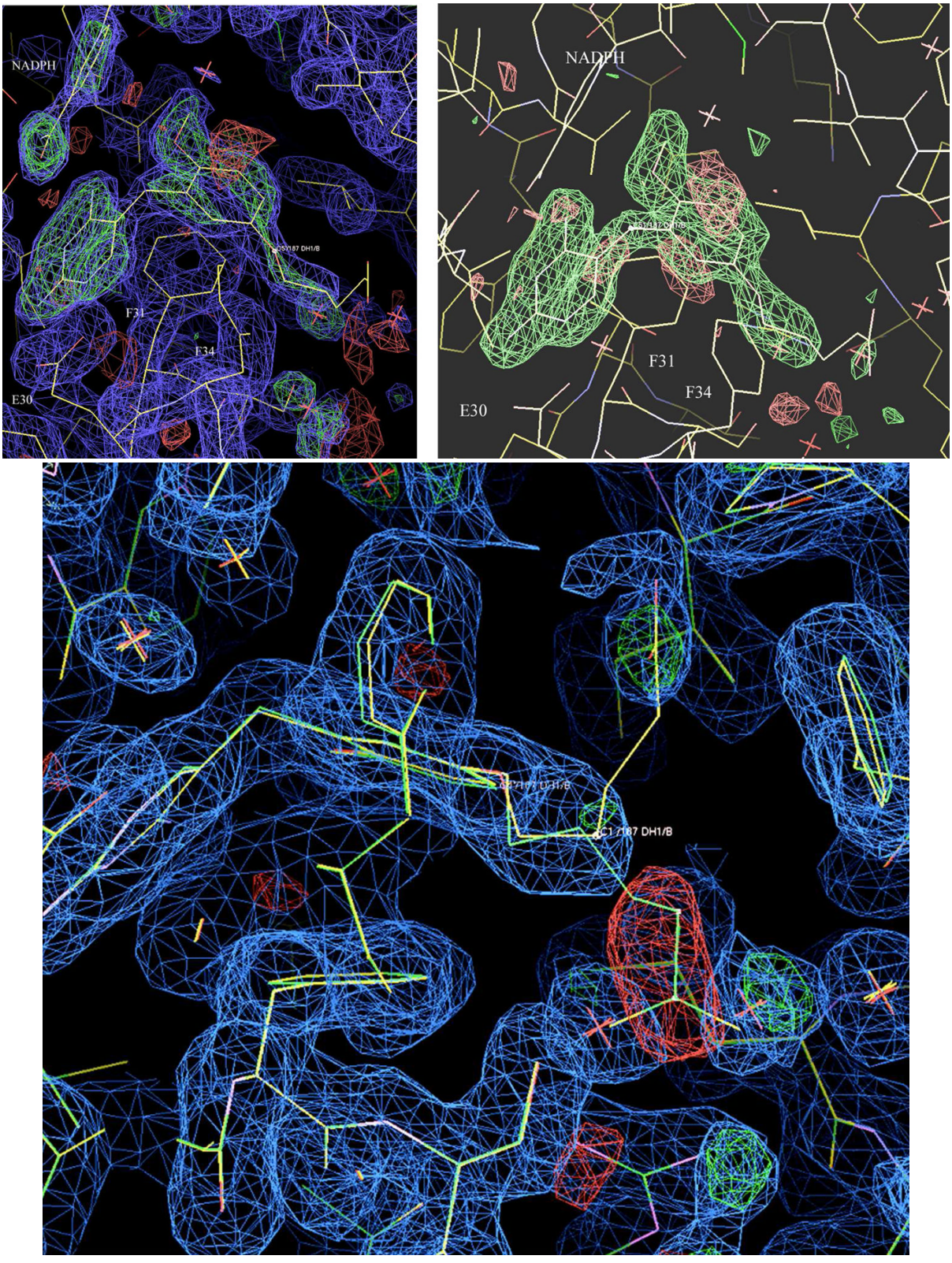

Figure 2.

Fig. 2. (left) 2Fo-Fc difference electron density map (0.8σ, blue; 3σ, green) showing the fit of the inhibitor PY957 and NADPH in the active site of Q35S/N64F human DHFR ternary complex with NADPH and PY957. The map was phased using only the enzyme hDHFR as the search model. (right) Omit map from final refinement showing Fo-Fc density for PY957 (3σ, green).

Fig. 2c. 2Fo-Fc difference electron density map (0.8σ, blue) showing the fit of the inhibitor PY957 in the active site of Q35S/N64F double mutant of human DHFR ternary complex with NADPH and PY957. Model of PY957 (green) in expected conformation interacting with Arg70 reveals negative (−3σ, red) density indicating that the side chain does not fit in this position. The correct model (yellow) indicates that water molecules interact with Arg70 while the side chain is folded such that it is between Phe31 and Phe64.

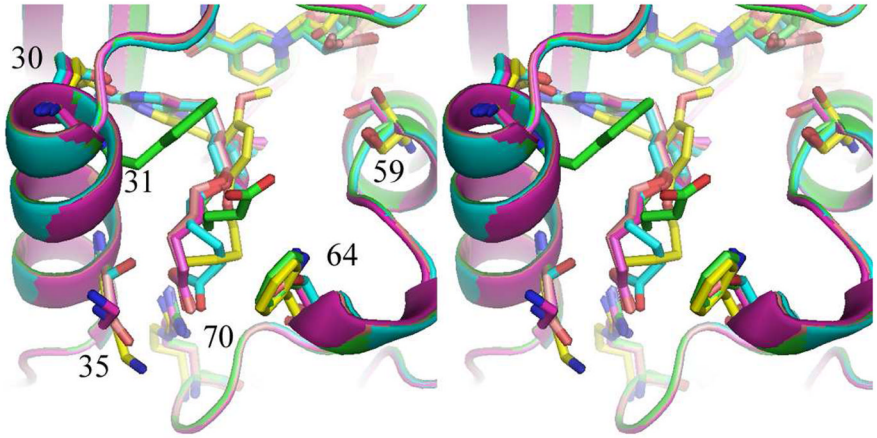

Fig. 3.

Stereo view of the superposition of the hDHFR NADPH PY957 ternary complexes with: Q35K (violet), the Q35S/N64S double mutant (cyan), the Q35S/N64F double mutant (green), wild type hDHFR (pink), and pcDHFR wild type NADPH PY957 ternary complex (yellow) (16). The wild type structure has nearly the same conformation as the single mutant protein. Figure was drawn with PyMol (33).

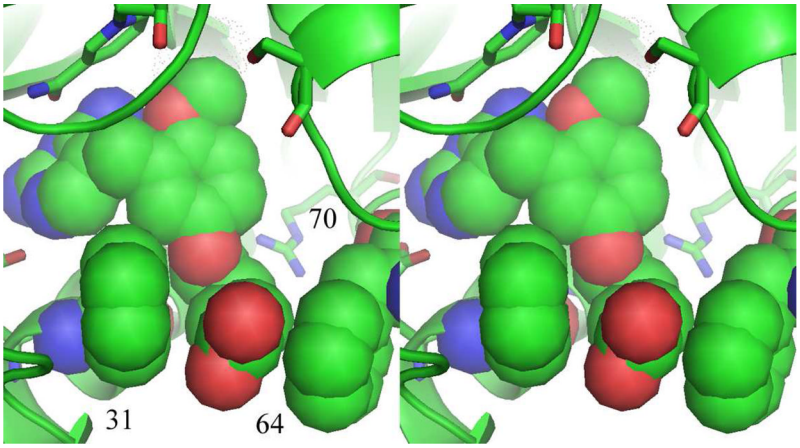

Fig. 4.

Stereo view of the interactions of PY957 side chain in the active site of the double mutant protein Q35S/N64F of hDHFR illustrating the hydrophobic contacts made between Phe31 and Phe64 of the mutant protein and the methylene carbons of the PY957 side chain. This conformation has the side chain flipped such that the carboxylate oxygen atoms no longer interact with Arg70 as observed in the other PY957 structures.

Table 1

Sequence alignment of human (h) (186 residues), *Pneumocystis carinii* (pc) and *Pneumocystis jirovecii* (pj) (both 206 residues) DHFR. Mutational sites are underlined and in red while key active site residues are numbered and colored cyan. CLUSTAL FORMAT for T-COFFEE Version_5.68 [http://www.tcoffee.org].

```
                                                30 31   35  38 39
hDHFR   --MVGSLNCIVAVSQNMGIGKNGDLPWPPLRNEFRYFQRMTT---TSSVEGKQNLVIMGK

pcDHFR MNQQKSLTLIVALTTSYGIGRSNSLPWK-LKKEISYFKRVTSFVPTFDSFESMNVVLMGR

pjDHFR MDWQKSLTLIVALTLSRGIGLKNDLPWK-LKSDMMFFSRVTSGLLVTRSTGQMNVVLMGR

           59 60 64    70
hDHFR   KTWFSIPEKNRPLKGRINLVLSRELKEPPQGAHFLSRSLDDALKLTEQ---PELANKVDM

pcDHFR KTWESIPLQFRPLKGRINVVITRNESLDLGNGIHSAKSLDHALELLYRTYGSESSVQINR

pjDHFR KTWESLPAHSRPLKNRINVVISRQEVLDLGGGAYHARSLDDALALLSQIYDSTSKIQLNR


hDHFR   VWIVGGSSVYKEAMNHPGHLKLFVTRIMQDFESDTFFPEIDLEKYKLLPEYPGVLSDVQ-

pcDHFR IFVIGGAQLYKAAMDHPKLDRIMATIIYKDIHCDVFFPLKFRDKEWSSVWKKEKHSDLES

pjDHFR VFVIGGGELYKAAMEHSRLNRIIATVIHNEVDCDVFFPIDFRSSQSCLPWRKQDHSVLEA

                                  186
hDHFR   -----------EEKGIKYKFEVYEKND

pcDHFR WVGTKVPHGKINEDGFDYEFEMWTRDL

pjDHFR WVGSKVPQGKINENGFIYEFEMWIRDI
```

Table 2

Kinetic constants for substrate and cofactor for pj-, pc- and hDHFR and its active site mutants that reflect human to *P neumocystis* changes.

Enzyme	K_m DHFA μM	K_m NADPH μM	k_{cat} sec^{-1}	k_{cat}/K_m DHFA $sec^{-1}\mu M$
pjDHFR	2.8 ± 0.04 (n=2)	22.9 ± 2.1* (n=2)	53 ± 4.2 (n=6)	19
pcDHFR	4.9 ± 0.3* (n=5)	14.5 ± 2.2 (n=2)	284 ± 13* (n=3)	58
pcDHFR K37Q	8.5 ± 0.87 (n=7)	9.2 ± 1.9 (n=1)	36 ± 2.4 (n=9)	4
hDHFR	2.7 ± 0.5 (n=4)	4.0 ± 1.8 (n=2)	40 ± 2.2 (n=8)	15
Mutants h→pjDHFR				
Q35S	1.1 ± 0.4 (n=4)	4.4 ± 2.0 (n=2)	35 ± 3.3 (n=4)	33
N64S	0.18 ± 0.06 (n=2)	6.3 ± 0.5 (n=1)	47 ± 5.3 (n=3)	261
Q35S/N64S	1.6 ± 0.4 (n=2)	4.6 ± 2.2 (n=2)	27 ± 4.5 (n=2)	17
Mutants h→pcDHFR				
Q35K	0.76 ± 0.2* (n=4)	13.0 ± 0.5 (n=2)	48 ± 4.0 (n=6)	63
N64F	0.81 ± 0.3* (n=3)	5.2 ± 2.8 (n=2)	40 ± 7.5 (n=3)	49
Q35K/N64F	0.49 ± 0.05* (n=4)	5.5 ± 1.8 (n=2)	43 ± 2.5 (n=4)	88

*Value is statistically different from the value for native human DHFR.

Table 3

Kinetic constants for selected antifolates against pjDHFR, pcDHFR, and wild type and mutant hDHFR.

Enzyme	TMP, nM K_i	MTX, nM K_i	PY957, nM K_i
pjDHFR	43 ± 5* (n=14)	0.042 ± 0.010 (n=13)	26.3 ± 7.4* (n=7)
pjDHFR (5)	28 ± 2 (n=2)	0.062 ± 0.013 (n=2)	
pcDHFR	800± 300* (n=7)	0.014 ± 0.004* (n=4)	21.9 ± 9.3* (n=7)
pcDHFR K37Q	75.0 ± 3.9 (n=5)	0.063 ± 0.4 (n=6)	7.6 ± 1.9 (n=6)
hDHFR	5200 ±700 (n=4)	0.093 ± 0.021 (n=8)	230 ± 20 (n=4)
Mutant h→pjDHFR			
hDHFR Q35S	1800 ± 100* (n=3)	0.047 ± 0.008 (n=3)	350 ± 130 (n=3)
hDHFR N64S	170 ± 0.5* (n=2)	0.003 ± 0.004* (n=2)	23 ± 14* (n=2)
hDHFR Q35S/N64S	1200 ± 100* (n=4)	0.047 ± 0.007 (n=4)	66 ± 2* (n=3)
Mutant h→pcDHFR			
hDHFR Q35K	390 ± 30* (n=2)	0.002 ± 0.0002* (n=2)	8.3 ± 0.4* (n=4)
hDHFR N64F	490 ± 160* (n=3)	0.029 ± 0.006* (n=3)	5.2 ± 1.6* (n=2)
hDHFR Q35K/N64F	650 ± 180* (n=5)	0.019 ± 0.006* (n=8)	13 ± 3* (n=2)

* Value is statistically different from the value for native human DHFR

Table 4

Data collection and refinement statistics for the wild type, single and double mutant proteins of human DHFR NADPH ternary PY957 inhibitor complexes.

Data collection	**Q35S/N64S -PY957**	**Q35S/N64D -PY957**	**-PY957**	**wt -PY957**
PDB accession #	3F8Y	3F87	3F91	3FS6
Space group	H3	H3	H3	H3
Cell dimensions (Å)				
a=b=	84.29	84.42	84.63	84.08
c =	78.12	77.93	77.92	78.06
Beamline	9-1 SSRL	RaxisIV	RaxisIV	9-2 SSRL
Resolution (Å)	53.34–1.45 (1.53)	26.22–2.01 (2.2)	26.70–1.90 (2.0)	53.2–1.2
Wavelength (Å)	1.00	1.5418	1.5418	1.00
Rmerge	0.039	0.071	0.048	0.07
R_{sym}(%) [a,b]	0.046	0.081	0.055	0.02
Completeness (%) [a]	99.1 (98.9)	97.0 (70.0)	99.5 (96.8)	100.0
Observed reflections	153,756	68,430	79,767	59,797
Unique reflections	50,420	17,593	20604	56,766
I/σ (I)	16.7 (6.1)	16.3 (1.3)	28.1 (9.0)	20.8
Multiplicity [a]	3.6 (3.0)	3.9 (1.7)	3.9 (1.7)	11.1
Refinement and model quality				
Resolution range (Å)	26.67–1.45	26.66–2.01	26.69–1.90	34.4–1.2
No. of reflections	34,546	12,666	15,480	56,766
R-factor [c]	19.0	16.1	18.5	24.5
R_{free}-factor [d]	22.8	21.9	24.2	26.0
Total protein & ligand atoms	1957	1871	1753	1642
Total water atoms	372	276	168	67
Average B-factor (Å^2)	18.9	19.9	12.5	16.0
Error in Luzzati plot	0.159	0.186	0.189	0.178
Rms deviation from ideal				
Bond lengths (Å)	0.010	0.018	0.016	0.009
Bond angles (°)	1.84	1.97	2.06	1.57
Ramachandran plot				
Most favored regions (%)	90.6	94.3	92.5	91.2
Additional allowed regions (%)	9.4	5.0	6.9	8.8
Generously allowed regions (%)	0.0	0.6	0.6	0.0
Disallowed regions (%)	0.0	0.0	0.0	0.0

[a] The values in parentheses refer to data in the highest resolution shell.

[b] $R_{sym} = \Sigma_h\Sigma_i|I_{h,i} - \langle I_h\rangle|/\Sigma_h\Sigma_i|I_{h,i}|$, where $\langle I_h\rangle$ is the mean intensity of a set of equivalent reflections.

[c] R-factor $= \Sigma|F_{obs} - F_{calc}|/\Sigma F_{obs}$, where F_{obs} and F_{calc} are observed and calculated structure factor amplitudes.

[d] R_{free}-factor was calculated for R-factor for a random 5% subset of all reflections.

Table 5

Bridge conformation for PY957 hDHFR complexes. Numbering scheme is shown in Figure 1.

Torsion Angle	hDHFR-Q35K-PY957	hDHFR-Q35S/N64S-PY957	hDHFR-Q35S/N64F PY957	pcDHFR-PY957	hDHFR-PY957
C4-C5-C51-C1′	−88.9°	-80.7°	−86.5°	179.1°	−88.7
C5-C51-C1′-C2′	97.2	96.5	100.3	−88.9	98.3
C51-C1′-C2′-O2′	−1.1	−1.4	−3.5	0.1	−1.4
C1′-C2′-O2′-C21	124.5	168.4	163.4	−115.8	140.5
C4′-C5′-O51-C52	78.5	85.0	−69.9	51.0	−101.5
C51′-O51-C52-C53	152.0	157.8	141.0	163.4	150.7
O51-C52-C53-C54	−154.1	−48.5	68.1	39.2	−142.6
C52-C53-C54-C55	141.1	−60.9	−112.7	63.6	140.9
C53-C54-C55-C56	−115.6	−64.7	159.9	49.8	−126.2
C54-C55-C56-O7	177.6	−77.9	−133.3	−118.1	176.2